https://doi.org/10.5194/essd-2021-279
Preprint. Discussion started: 16 December 2021

Open Access Earth System Science Data Discussions

A temporally consistent 8-day 0.05° gap-free snow cover extent dataset over the Northern Hemisphere for the period 1981–2019

Xiaona Chen[1], Shunlin Liang[2], Lian He[3], Yaping Yang[1], and Cong Yin[1, 4]

[1]State Key Laboratory of Resources and Environmental Information System, Institute of Geographic Sciences and Natural Resources Research, Chinese Academy of Sciences, Beijing, 100101, China
[2]Department of Geographical Sciences, University of Maryland, College Park, 20740, USA
[3]School of Geospatial Engineering and Science, Sun Yat-Sen University, Zhuhai, 519082, China
[4]College of Resources and Environment, University of Chinese Academy of Sciences, Beijing, 100049, China

Correspondence to: Xiaona Chen (chenxn@igsnrr.ac.cn)

Abstract. Northern Hemisphere (NH) snow cover extent (SCE) is one of the most important indicator of climate change due to its unique surface property. However, short temporal coverage, coarse spatial resolution, and different snow discrimination approach among existing continental scale SCE products hampers its detailed studies. Using the latest Advanced Very High Resolution Radiometer Surface Reflectance (AVHRR-SR) Climate Data Record (CDR) and several ancillary datasets, this study generated a temporally consistent 8-day 0.05° gap-free SCE covering the NH landmass for the period 1981–2019 as part of the Global LAnd Surface Satellite dataset (GLASS) product suite. The development of GLASS SCE contains five steps. First, a decision tree algorithm with multiple threshold tests was applied to distinguish snow cover (NHSCE-D) with other land cover types from daily AVHRR-SR CDR. Second, gridcells with cloud cover and invalid observations were filled by two existing daily SCE products. The gap-filled gridcells were further merged with NHSCE-D to generate combined daily SCE over the NH (NHSCE-Dc). Third, an aggregation process was used to detect the maximum SCE and minimum gaps in each 8-day periods from NHSCE-Dc. Forth, the gaps after aggregation process were further filled by the climatology of snow cover probability to generate the gap-free GLASS SCE. Fifth, the validation process was carried out to evaluate the quality of GLASS SCE. Validation results by using 562 Global Historical Climatology Network stations during 1981–2017 (r=0.61, p<0.05) and MOD10C2 during 2001–2019 (r=0.97, p<0.01) proved that the GLASS SCE product is credible in snow cover frequency monitoring. Moreover, cross-comparison between GLASS SCE and surface albedo during 1982–2018 further confirmed its values in climate changes studies. The GLASS SCE data are available at https://doi.org/10.5281/zenodo.5775238 (Chen et al. 2021).

1 Introduction

Season snow cover is the largest component of the cryosphere and has been designated as one of the Essential Climate Variables (ECVs) of the Global Climate Observing System (GCOS) due to its high surface albedo, heat insulation, and

https://doi.org/10.5194/essd-2021-279
Preprint. Discussion started: 16 December 2021

contribution to soil moisture and runoff (GCOS, 2019b; Bojinski et al., 2014). The global mean winter maximum snow cover extent (SCE) is about 47×10^6 km², in which 98% is distributed in the Northern Hemisphere (NH) (NSIDC, 2019). Therefore, NH snow cover is highly concerned by the International Panel on Climate Change (IPCC) (Hock et al., 2019) and World Meteorological Organization (WMO) (WMO, 2020), and plays a crucial role in the Earth's climate system through the surface energy budget (Flanner et al., 2011; Chen et al., 2016; Thackeray and Fletcher, 2016; Chen et al., 2015), atmospheric circulation (Henderson et al., 2018), as well as hydrological cycle (Immerzeel et al., 2019; Barnett et al., 2005; Pulliainen et al., 2020), and influences freshwater resources across a large proportion of the NH, especially in the mountain regions (Barnett et al., 2005).

Accurate information on SCE in NH is vital not only for an improved understanding of the role that snow cover plays in the Earth climate system but also for disaster prevention for several reasons. First, snow cover has important linkages with large-scale climate system anomalies through its influence on surface energy (Flanner et al., 2011; Chen et al., 2015; Chen et al., 2016). The shrinkage of SCE reduces the reflection of Earth surface, results in additional absorbed solar radiation in Earth-Atmosphere system, and leads to rising surface air temperatures (Qu and Hall, 2014). Thus, the presence or absence of snow cover controls patterns of heating and cooling over Earth's surface more than any other land cover types. Second, SCE is sensitive to both climate change on long-term and weather on short-term. For example, snow cover is proved to be closely related with several climate anomalies, such as vegetation phenology (Chen and Yang, 2020; Peltoniemi et al., 2018), monsoons (Boos and Kuang, 2010), river sediment (Nie et al., 2015), livelihoods (Haynes et al., 2014), and sea ice thickness (Mallett et al., 2021). Third, snow cover has great potential to influence the regional hydrological cycle and results in subsequent ecosystem anomalies. For example, decrease in spring SCE in Tibetan Plateau is contribute to advance in vegetation greenness onset (Dong et al., 2013) and dynamics of vegetation growth (Wang et al., 2018). Moreover, early snowmelt significantly enhances boreal springtime carbon uptake (Pulliainen et al., 2017). Fourth, snow cover also supporting lives (Immerzeel et al., 2019). Seasonal snow cover across the Tibetan Plateau constitutes vital surface water storage for Southwest China and neighboring Asian countries, and sustains more than one billion people in Asia. Last, abnormal snowmelt in spring and snowfall in winter are being a serious threat to water resource sustainability and social-economic development, such as agricultural production damage (Qin et al., 2020), spring flooding (Diffenbaugh et al., 2013), as well as building collapse, road congestion, and avalanches.

Because of above mentioned significances of SCE, the scientists have given considerable consideration to map and monitor SCE since 1960s. Compared with traditional field snow surveying, satellite remote sensing has distinct advantages in SCE mapping, such as large spatial coverage, fine spatial resolution, high temporal resolution, and economical and practical in application (Yang et al., 2013; Frei et al., 2012). Several published SCE datasets are available in climate change studies, as listed in Table 1, including the binary daily snow cover mask derived from the Interactive Multi-sensor Snow and Ice Mapping System (IMS) (Helfrich et al., 2007), the Northern Hemisphere Weekly Snow Cover and Sea Ice Extent (NHSSCE) (Brodzik and Armstrong, 2013), the Moderate-Resolution Imaging Spectroradiometer (MODIS) snow cover products in Climate Modeling Grid (CMG) (Hall et al., 1995), the Suomi National Polar-orbiting Partnership (NPP) Visible Infrared Imaging Radiometer

https://doi.org/10.5194/essd-2021-279
Preprint. Discussion started: 16 December 2021


Open Access Earth System Science Data Discussions

Suite (VIIRS) CMG snow cover product (Key et al., 2013), the European Space Agency (ESA) Global Snow Monitoring for Climate Research (GlobSnow) (Pulliainen, 2006), the ESA Snow Climate Change Initiative (CCI) global daily snow viewable on top of the forest canopy (SCFV) (Naegeli et al., 2021a) and snow cover fraction on ground (SCFG) (Naegeli et al., 2021b) from MODIS and Advanced Very High-Resolution Radiometer (AVHRR) sensors, the long-term NH daily 5-km SCE product (JASMES) (Hori et al., 2017), and the snow water equivalent products from the Advanced Microwave Scanning Radiometer-Earth Observing System (Kelly et al., 2003) and GlobSnow (Pulliainen, 2006). Based on the above mentioned SCE dataset, continental scale snow cover anomalies in coarse spatial resolution have been quantified in published studies.

However, compared with other components at the land surface, the cryosphere, including snow cover, is still one of the most under-sampled domains of the Earth system (WMO, 2020). The existing continental scale snow cover dataset are summarized in Table 1. Although satellite remote sensing has been employed in SCE monitoring for several decades, the limitations of public SCE dataset, such as incomplete spatial coverage (*e.g.*, MODIS CMG, VIIRS CMG, JASMES, ESA SCFG and SCFV), short time span (*e.g.*, VIIRS CMG, GlobSnow SE, and IMS), and low spatial resolution (*e.g.*, NOAA NHSCE-CDR, NHSSCE, and MEaSUREs NHSCE) still pose great challenges in capturing the robust long-term trends of snow cover variables and largely restrict their application in climate change. In particular, SCE studies prior 2000 are mainly based on NOAA NHSCE-CDR at 100km spatial resolution and NHSSCE at 25 km spatial resolution. In spite of JASMES, ESA snow CCI SCFG and SCFV have provide daily SCE at 5km spatial resolution before 2000, the tremendous gaps caused by invalid observations, cloud contamination, and limited track coverage still hampered their application in hemispheric SCE studies.

To serving studies in snow cover, climate change, and monitoring snow related activities, such as the detection of variability and trends, climate modelling, and applications of hydrology, meteorology, and biology, a usability long-term series, temporally consistent, and gap-free SCE data set is needed. Accordingly, the objective of the present study was to develop an 8-day gap-free terrestrial SCE over the NH as a new member of the Global LAnd Surface Satellite (GLASS) products suite (Liang et al., 2021). To achieve this objective, we executed five tasks. First, we generate a NH daily 5-km SCE record (NHSCE-D) using the National Oceanic and Atmospheric Administration (NOAA) Climate Data Record (CDR) of AVHRR Surface Reflectance (AVHRR-SR CDR), Version 5 (Vermote et al., 2019) though a decision tree approach. Second, we merged NHSCE-D with JASMES and ESA SCFG to develop a combined daily SCE over the NH (NHSCE-Dc). Integration or combination of multiple products is a new trend in satellite product generation (Liang et al., 2018; Muhammad and Thapa, 2020; Gascoin et al., 2019). Compared with other published snow cover products, JASMES, ESA SCFG, and ESA SCFV are available longterm daily SCE derived from AVHRR images in finer spatial resolution (5km). To take advantage of their temporal consistence and fill gaps in NHSCE-D, both JASMES and ESA CCI SCFG are employed in the combination process. Since ESA CCI SCFV focus on viewable daily snow cover fraction from space on top of the land surfaces instead of ground, it was excluded in the combination process. Third, to remove the remaining gaps and improve the spatial integrity, we aggregated NHSCE-Dc in each 8-day period to get the maximum SCE (NHSCE-8Dc) and minimum gaps in each 8-day period. Fourth, the resting gaps in NHSCE-8Dc were further filled by the 8-day climatology of snow cover probability to develop the

https://doi.org/10.5194/essd-2021-279
Preprint. Discussion started: 16 December 2021

8-day gap-free GLASS SCE. The spatial and temporal complete IMS in 4 km spatial resolution during 2005–2019 was employed to calculate the 8-day climatology of snow cover probability for each gridcell. Finally, independent variables form the Global Historical Climatology Network (GHCN) daily snow depth observations, 8-day MODIS CMG products (MOD10C2), and the CLoud, Albedo and surface RAdiation dataset from AVHRR data Edition 2a surface albedo (CLARA-A2-SAL) were employed in the validation and quality assessment analysis. The datasets used in this study are introduced in section 2. The detained methods for GLASS SCE development is presented in Section 3. The results are displayed in Section 4. The discussion and conclusions are given in Section 5.

2 Datasets

To illustrate the process of GLASS SCE generation, datasets used for NHSCE-D generation, existing SCE data sets used in combination and integration, independent variables used for validation and cross-comparison analysis were described separately in this section.

2.1 Data sets used for NHSCE-D generation

The AVHRR-SR CDR, the Terra and Aqua combined MODIS land cover climate modeling grid (MCD12C1), and elevation data are key input variables of NHSCE-D generation.

2.1.1 AVHRR-SR CDR

The AVHRR-SR CDR gridded daily surface reflectance and brightness temperatures derived from the AVHRR sensors onboard eight NOAA polar orbiting satellites, including NOAA-7, NOAA-9, NOAA-11, NOAA-14, NOAA-16, NOAA-17, NOAA-18, and NOAA-19 at 0.05° spatial resolution spans from 1981 to the present (Vermote et al., 2019), which is the best data source for large-scale and longterm snow mapping, especially for years before 2000. The spectral bands of AVHRR-SR CDR are listed in Table 2. The quality control (QA) descriptions are summarized in Supplementary Table S1.

Compared with AVHRR images used in previous studies, such as Hori et al. (2017) and Zhou et al. (2013), the AVHRR-SR CDR has calibrates different NOAA polar orbiting instruments and provides consistent global daily average surface reflectance and brightness temperatures, which facilitates their application in longterm snow cover mapping. Evaluation results of the AVHRR-SR CDR in the monitoring of United States wheat yield (Franch et al., 2017) and gap-free daily SCE generation over the Tibetan Plateau (Chen et al., 2018) demonstrated that the AVHRR-SR CDR were reliable in mapping of longterm terrestrial surface variables. Therefore, for purpose of the present study, the daily AVHRR-SR CDR for the period 1981–2019 at 0.05° spatial resolution is employed as the primary input data for GLASS SCE generation.

https://doi.org/10.5194/essd-2021-279
Preprint. Discussion started: 16 December 2021

2.1.2 MCD12C1 land cover dataset

To increase the snow discrimination accuracy from the AVHRR-SR CDR, the development of NHSCE-D was initiated within the MCD12C1 International Geosphere Biosphere Program (IGBP) land cover types in year of 2019 at 0.05° spatial resolution. The MCD12C1 IGBP classification divides the global land surface into 17 types, including 11 natural vegetation types, 3 land use related types, and 3 vegetation-free land types (Friedl and Sulla-Menashe, 2015). To increase the snow cover discriminating accuracy among different land cover types, we re-classified the NH land cover into four types cording to the IGBP classification (Supplementary Table S2), i.e., (1) forests and shrublands, (2) grasslands, (3) barren land, and (4) permanent snow and ice. The forests and shrublands include evergreen needle-leaf forest, evergreen broad-leaf forest, mixed forest, closed shrublands, open shrublands, and woody savannas, the grasslands, include cropland/natural vegetation, grasslands, and cropland, the barren lands include barren and sparsely vegetated, urban, and built-up. , and the permanent snow and ice types equal to the types defined by the IGBP classification scheme.

2.1.3 Elevation dataset

To detect cloud cover before the snow detection process, an auxiliary global 1-km resolution land surface digital elevation model (DEM) derived from the 30 arc-second NASA Shuttle Radar Topography Mission (SRTM30) (Becker et al., 2009) was used in this study.

2.2 Datasets used for combination and integration

Due to gaps caused by track, swath, solar zenith angle, view zenith angle, and cloud contamination of original AVHRR images, the spatial coverage of snow cover datasets retrieved from daily AVHRR observations are inevitable incomplete in spatial coverage. To fill gaps in NHSCE-D, published daily SCE products retrieved from AVHRR observation using different algorithms including JASMES, ESA SCFG were employed in the combination analysis. Moreover, to exclude the influence of bright surface in snow cover detection and fill resting gaps after the combination process, the spatial and temporal complete IMS was also used in the combination and integration analysis.

2.2.1 JASMES daily SCE dataset

The JASMES daily SCE dataset was developed by the application of a consistent objective snow cover mapping algorithm based on the historical optical sensors on NOAA polar orbiting satellites for the period 1978–2019, including AVHRR GAC radiance data during 1978–2019, and MODIS radiance data during 2000–2019 (Hori et al., 2017). The estimation results of unbiased JASMES SCEs using long-term NOAA SCE have endorsed the performance of JASMES in snow mapping (Hori et al., 2017). Due to systematic bias between AVHRR GAC and MODIS radiance data may influence the consistency of JASMES in snow cover detection, this study only used SCE retrieved from the AVHRR GAC radiance data.

2.2.2 ESA SCFG daily SCF dataset

https://doi.org/10.5194/essd-2021-279
Preprint. Discussion started: 16 December 2021

The ESA SCFG provides global daily SCF on ground from AVHRR for the period 1982–2019 at 0.05 spatial resolution (Naegeli et al., 2021b). The retrieval method of the ESA SCFG product is originates from the ESA GlobSnow approach described in Metsämäki et al. (2015) and complemented with a pre-classification module. All cloud free pixels are then used for the snow extent mapping, using spectral bands centered at about 630 nm and 1.61 µm, and an emissive band centered at about 10.8 µm. similar with JASMES, the spatial coverage of ESA CCI SCFG is also incomplete. Since the ESA CCI SCFG is a newly released dataset, the

2.2.3 IMS daily SCE products

The IMS provides daily binary snow cover mask created manually by a snow analyst approach, which enables qualified analysts to access multiple sets of remotely sensed data in order create and distribute maps of snow and ice at three different resolutions (1 km, 4 km, and 24 km) across the NH (Nsidc, 2008). However, short temporal coverage limits its application in longterm climate studies. Therefore, we employed IMS in snow cover probability calculation instead of combining with NHSCE-D. To obtain snow cover probability at comparable spatial resolution with NHSCE-D at 0.05°, the IMS at 4-km spatial resolution for the period 2005–2019 was used in the analysis. For a given gridcell, the snow cover probability was calculated by the number of years with snow cover divided by the number of years. The daily rate of agreement between the IMS snow maps and ground snow observations between 2006 and 2010 ranged mostly between 80% and 90% through winter seasons over Continental United States (Chen et al., 2012). Moreover, the IMS has been used to generate gap-free SCE over the NH because of complete spatial coverage and high temporal resolution (Chen et al., 2021).

2.3 Data sets used for validation and cross-comparison analysis

To verify the reliability and performance of GLASS SCE in snow cover mapping over the NH, GHCN daily snow depth observation, objective MOD10C2, and CLARA-A2 land surface albedo dataset were used in the analysis.

2.3.1 GHCN daily snow depth observations

By assembling and checking observations made in multiple different nations, the GHCN provides daily snow depth records from over 75,000 stations in 180 countries and territories (Menne et al., 2012). For purpose of the present study, 562 GHCN stations over the NH covering 1982 to 2017 were selected in the analysis. The distribution of the selected GHCN stations is displayed in Figure 1.

Missing records of daily snow depth were filled by using accompanied daily surface air temperature and daily precipitation according to Yuan et al. (2016) and Xu et al. (2017). When the missing records were less than 15 consecutive days, if the daily average surface air temperature was below 0°C, then daily precipitation was added to the daily snow depth, and if the daily average air temperature was between 0°C and 2°C, then half of the precipitation was added to the daily snow depth.

2.3.2 MOD10C2 8-day snow cover fraction products

The MOD10C2 reports the 8-day percentage of snow-covered land globally at 0.05° spatial resolution since 2000 (Hall and Riggs, 2016). The 8-day composite is considered useful because persistent cloudiness limits the number of days available for

https://doi.org/10.5194/essd-2021-279
Preprint. Discussion started: 16 December 2021

surface observations in many regions, particularly at high latitudes (Frei et al., 2012). In this study, the MOD10C2 were used to verify the performance of newly developed GLASS SCE after 2000, because MOD10C2 is the only consistent, objective snow estimate derived from optical satellite observations with finer spatial resolution compared with AVHRR retrieved GLASS SCE. For purpose of the present study, the MOD10C2 during 2000−2019 were employed in the analysis. Moreover, missing SCF values in MOD10C2 were filled by the climatology of SCF calculated from IMS during 2005−2019.

2.3.3 CLARA-A2-SAL surface albedo data

Surface albedo is defined as the ratio of the reflected radiation flux to the incoming radiation flux, which is a key forcing parameter controlling the partitioning of radiative energy between the atmospheric and surface and has also been designed as one of the ECVs (Gcos, 2019a). The CLARA-A2-SAL is generated based on a homogenized AVHRR radiance time series and is created by using algorithms to derive surface albedo for different land use areas separately, which is the only available long time-span albedo product derived from AVHRR imagery (Karlsson et al., 2017). Changes in snow cover have been shown to be related closely with anomalies in land surface albedo because of its high reflectance (Chen et al., 2015).Therefore, the independent long-term CLARA-A2-SAL for the period 1982−2019 at a spatial resolution of 0.25° was used to compare with the spatiotemporal variability in snow cover calculated from the GLASS SCE in this study.

2.4 Data preparing

Details of datasets used in this study are listed in Table 3. Abbreviations used in this study is listed in appendix Table 1.

To match the spatial resolution of the AVHRR-SR CDR, datasets used in this study were regridded at a spatial resolution of 0.05° and an array resolution of 7200 × 1800 gridcells with the geographic projection. The geographic coordinates of the upper-left gridcell are 90.0°N latitude and -180.0° longitude. The geographic coordinates of the lower-right gridcell are 0° latitude, 180.0° longitude. For datasets with spatial resolution finer than 0.05°, we used "average" in the resampling process, which computed the weighted average of all non-NODATA contributing pixels in the domain of our study. For datasets with spatial resolution coarser than 0.05°, we used "cubic-spline" in the resampling process.

3 Methodology

The flowchart of GLASS SCE generation is presented in Figure 2. First, by using the quality control flag (Supplementary Table S1), gridcells with valid observations in channels 1–5 of AVHRR-SR CDR were chosen in the subsequent analysis. Second, the cloud detection was carried out to distinguish cloud cover with other land surface types. Third, the NHSCE-D was retrieved from resting gridcells of AVHRR-SR CDR by using a decision tree approach. The decision tree and threshold values for snow mapping are listed in Figure 2. Fourth, the NHSCE-D were combined with JASMES and ESA SCFG to fill the gaps caused by invalid observations and cloud cover. Fifth, the NHSCE-Dc was aggregated to produce an 8-day maximum SCE over the NH (NHSCE-8Dc) to improve the spatial integrity of NHSCE-Dc. Finally, remaining gaps in NHSCE-8Dc were filled by using the snow cover probability to generate a spatial complete gap-free GLASS SCE.

https://doi.org/10.5194/essd-2021-279
Preprint. Discussion started: 16 December 2021

3.1 Quality control and invalid observations detection

By using the quality control flag (Supplementary Table S1), grid cells with valid observations in channels 1–5 were selected in NHSCE-D generation, in which only the quality control flags of "1" in bit 7, indicating channels 1–5 of AVHRR-SR CDR are valid were chosen in the subsequent analysis. Moreover, to reduce the error in snow detection caused by distortions in pixel geometry, only gridcells with a view zenith angle of less than 45° were used in this study.

3.2 Cloud cover detection

Previous studies have reported that the cloudy flag in AVHRR-SR CDR appears to overestimate cloudy pixels compared with traditional cloud detection (Chen et al., 2018). Therefore, we did not adopt the cloudy and cloud shadow flag that accompanies the AVHRR-SR CDR. To resolve this issue, we employed the cloud detection test and threshold values (Supplementary Table S3) according to Hori et al. (2017), as listed in Supplementary Table S3.

3.3 Snow cover mapping

A decision tree was employed to classify the land surface over the NH into snow and non-snow. Based on the MODIS IGBP land cover classification, gridcells in study area were reclassified into four types at the beginning of the snow cover detection process. The variables and thresholds for snow and non-snow classification applied in the decision tree are shown in Figure 3, in which the NHSCE-D is defined as the combination of Snow-01 to Snow-04.

The snow-covered area is often estimated by using optical satellite information in combination with the normalized-difference snow index (NDSI) by referring to the normalized-difference vegetation index (NDVI), particularly in dense vegetation regions (Hall et al., 1995). The NDSI thereby uses a threshold for the definition if a satellite pixel is assumed to be snow and non-snow. Most of these threshold values in snow cover detection were combinations of the conventional snow detection tests employed in polished studies, including Khlopenkov and Trishchenko (2007), Kidder (1987), Zhou et al. (2013), and Hori et al. (2017). Moreover, they have been applied in hemispherical SCE mapping with good applicability (Hori et al., 2017).

The spatiotemporal representativeness of the standard NDSI threshold of 0.4 (Hall et al., 1995) is questionable at the local scale, such as Zhang et al. (2019) and Zhou et al. (2013). However, according to Härer et al. (2018), using the standard NDSI threshold of 0.4 is adequate for satellite products with a pixel size of 500 m and more. For higher-resolution snow cover mapping, significant improvements in the quality of the snow cover maps can be achieved if a threshold is used which is variable in space and time. For snow cover mapping in coarse spatial resolution with a pixel size of 500 m or greater, the advantage of a location-dependent NDSI threshold vanishes. Usually, the NDSI was measured by using the red (0.63 μm) and shortwave infrared (1.64 μm) bands. As there are no shortwave infrared observations around the 1.64 μm in the AVHRR-SR CDR, we used the reflectance at 3.7 μm for an NDSI-like calculation and adopt 0.80 as the NDSI-like threshold in snow cover mapping process, following Hori et al. (2017).

https://doi.org/10.5194/essd-2021-279
Preprint. Discussion started: 16 December 2021

3.4 Composition process

To improve the spatial coverage and reduce the omission error of the NHSCE-D, a composition process was carried out to fill gaps caused by invalid observations and cloudy pixels. Two existing daily snow cover products retrieved from AVHRR images, including JASMES and ESA SCFG were used in the composite procedure. First, the gaps in NHSCE-D were filled by JASMES and ESA SCFG to produce a preliminary daily gap-filled NHSCE (NHSCE-G1). Second, the NHSCE-G1 was merged with NHSCE-D to generate a combined daily SCE over the NH (NHSCE-Dc). Using NHSCE-Dc in GLASS SCE development will reduce the omission error in individual SCE dataset.

3.5 Aggregation process

Subject to limited valid observations in AVHRR images, the spatial coverage of NHSCE-Dc is still incomplete. To improve the usability of NHSCE-Dc in climate change studies and match the temporal resolution of MODIS snow cover products after 2000, the NHSCE-Dc and rest gaps (Gaps-A) were first aggregated at each 8-day period to generate an 8-day maximum SCE (NHSCE-8Dc) and an 8-day minimum gaps (Gaps-B). The 8-day periods are listed in Supplementary Table S4. Then, the Gaps-B were filled by the climatology of 8-day snow cover probability calculated from the spatially complete IMS dataset during 2005–2019. For each gridcells covered by Gaps-B, the climatology of snow cover probability was employed to discriminate snow from non-snow, in which only the snow cover probability >50% was flagged as snow (NHSCE-G2) in the gap-filling process. Finally, the NHSCE-G2 were merged with NHSCE-8Dc to generate a spatial complete gap-free GLASS SCE.

3.6 Accuracy assessment of GLASS SCE

The GHCN daily snow depth records and MOD10C2 were used in the accuracy assessment of GLASS SCE. Compared with the newly developed GLASS SCE, the GHCN daily snow depth observations and 8-day MOD10C2 represent consistent and objective snow estimates derived from ground measurements and satellite retrieves in finer spatial resolution, respectively.

To estimate the accuracy of the GLASS SCE, we used annual SCF as criteria in the validation analysis, in which the annual SCF was defined as the total number of frames with snow divided by the number of frames in a year. For each GHCN snow depth observation, we first extract the number of days with snow depth greater than 0 cm in each 8-day period of the year. Then, the stations with snow-covered days greater than 1 day were flagged as snow in a given 8-day period. Finally, the annual SCF was defined as the total number of frames with snow divided by the number of frames in a year. For MOD10C2, we calculated the annual SCF by averaging all frames in a year.

The root-mean-square error (RMSE) and bias were used as criteria to evaluate the relative precision of GLASS SCE (X_i) to GHCN stations or MOD10C2 (Y_i) during their overlapping periods. The RMSE and bias of X_i relative to Y_i are calculated following Eq. (1) and Eq. (2), respectively:

https://doi.org/10.5194/essd-2021-279
Preprint. Discussion started: 16 December 2021


Open Access Earth System Science Data Discussions

$$RMSE = \sqrt{\frac{1}{n}\sum_{i=1}^{n}(X_i - Y_i)^2}\ , \quad (1)$$

$$Bias = \frac{1}{n}\sum_{i=1}^{n}(X_i - Y_i)\ , \quad (2)$$

where X_i is the SCF of grid cell *i* calculated from GLASS SCE, Y_i is the referencing SCF of grid cell *i* calculated from GHCN stations or MOD10C2.

4 Results

To verify the feasibility of GLASS SCE in climate change studies, we first estimated the relative accuracy of GLASS SCE to GHCN snow depth observations and MOD10C2. Then, we cross-compared GLASS SCE-retrieved SCF with GLARA-A2-SAL surface albedo in further.

4.1 Validating of GLASS SCE by using GHCN snow-depth observations

In situ GHCN snow depth observations are used to verify the performance of GLASS SCE to capture the distribution of "ground truth" SCF in this study. Limited by the temporal coverage of GHCN snow depth observation, the comparison between annual SCF calculated from GHCN and GLASS SCE was carried out for the overlapping period 1982–2017. Moreover, due to missing observations of AVHRR-SR CDR in late 1994, the year of 1994 is excluded in the analysis. The spatial patterns of the 35-year averaged SCF over the NH calculated form GHCN snow depth stations and GLASS SCE for the period 1982–2017 are displayed in Figure 4.

As shown in Figure 4, there are clear latitudinal gradient patterns for 35-year annual SCF from NH middle to high latitudes in both GHCN-observed SCF (Figure 4a) and GLASS SCE-retrieved SCF (Figure 4b), with low SCF values distributed in middles latitudes, but high SCF values occurred in high latitudes and high altitudes regions. The 35-year averaged annual SCF calculated from 562 GHCN snow depth observations is 38.14% (± 8.19%) for the period 1982–2017. Comparably, the value from GLASS SCE is 47.66% (± 15.76%) at the same time span.

The detailed comparison between 35-year averaged annual SCF calculated from GHCN snow depth stations and GLASS SCE (GLASS SCE-based SCF minus GHCN-observed SCF) over the NH for the period 1982–2017 (without 1994) are shown in Figure 5. The spatial distribution of differences indicate a better performance of GLASS SCE in low latitudes compared with high latitudes around the northern Europe and high altitudes around Chersky Mountains in Russia (Figure 5a). In most sites, the GHCN-observed SCF are consistent with the GLASS SCE-retrieved SCF, in which the linear correlation coefficient (*r*) varies as 0.61 at the 95% significant level (Figure 5b). However, the value of GLASS SCE-retrieved SCF are much higher than the GHCN-observed SCF, especially in rare snow distributed regions, in which the RMSE and bias between GLASS SCE-retrieved SCF and GHCN-observed SCF are 16.05% and 9.19%, respectively.

https://doi.org/10.5194/essd-2021-279
Preprint. Discussion started: 16 December 2021

The distribution of annual SCF differences (Figure 5c) explored that the GHCN stations with positive bias account for 81.18% of the total stations employed in this study, in which the differences between 5–10%, 10–15%, and >20% account for 22.58%, 18.10%, and 18.10% of the GHCN stations, respectively. Meanwhile, the GHCN stations with negative bias account for 18.82% of the total stations used in this study, which are mainly distributed in low to middle latitudes of North America.

Subjected to limited spatial representation of GHCN stations, the GHCN-observed SCF would give results that are highly dependent on particular locations (latitude and elevation). Such results would mostly reflect those accidental circumstances rather than yield meaningful information about the climate (Hansen et al., 2010). Therefore, the current differences between GLASS SCE-retrieved SCF and GHCN-observed SCF are reasonable in snow-related studies. Even though, the GLASS SCE-based SCF still skillfully captures SCF over the NH calculated from GHCN observations, which proves that the GLASS SCE approach used in our study is reliable.

4.2 Validating of GLASS SCE by using MOD10C2

The comparison between annual SCF calculated from GLASS SCE and MOD10C2 was carried out for the overlapping period 2001–2019. The 19-year averaged annual SCF calculated from MOD10C2 and GLASS SCE are shown in Figure 6. There are similar latitudinal and altitudinal gradient for annual SCF over the NH in both MOD10C2-retriebed SCF (Figure 6a) and GLASS SCE-retrieved SCF (Figure 6b). The 19-year averaged annual SCF over the NH calculated from GLASS SCE and MOD10C2 are 21.03% (±26.17%) and 20.62% (±25.14%) for the period 2001–2019. The annual SCF below 10% are mainly distributed in low latitudes United States and Eurasia. Compared with MOD10C2-retriebed annual SCF, the low SCF values in north margin of Africa and South America are not displayed in GLASS SCE-retrieved SCF maps. This is mainly caused by the 8-day climatology of snow cover probability used in the GLASS SCE generation.

The spatial distribution of differences between 19-year averaged annual SCF over the NH calculated form GLASS SCE and MOD10C2 (GLASS SCE-based SCF minus MOD10C2-based SCF) for the period 2001–2019 are shown in Figure 7. Compared with MOD10C2-based SCF, the GLASS SCE-retrieved SCF displayed a generally greater values in high latitudes regions and a lower values in low to middle latitudes over the NH. The detailed distribution of differences further demonstrated that most of the gridcells have a positive bias over the NH (figure 7c), in which the negative bias beyond -1% only account for 21.17% of the total gridcells. In comparison, the positive bias ranged from 1–5% and 5–10% account for 31.15% and 21.49% of the total gridcells, which represents the major differences distribution intervals.

The results from scatter plots (Figure 7b) indicated that the SCF calculated from GLASS SCE and MOD10C2 are tightly correlated over the NH for the period 2001–2019, with r varies as 0.97 at the 95% significant level, accompanied with RMSE and bias varies as 2.05% and 5.82%, respectively. Therefore, the GLASS SCE has comparable performance with MOD10C2 over the NH for the period 2001–2019.

https://doi.org/10.5194/essd-2021-279
Preprint. Discussion started: 16 December 2021

4.3 Cross-comparison between GLASS SCE and CLARA-A2-SAL

To further verify the performance of GLASS SCE in climate changes studies, this study focuses on the melting season of the snow cover (April–August) over the NH, which contains the most interesting albedo dynamics, similar with Riihelä et al. (2013). The cross-comparison between April–August averaged annual SCF and surface albedo over the NH during 1982–2018 was conducted, as shown in in Figure 8.

The distribution of 37-year mean of April–August averaged land surface albedo across the NH during 1982–2018 is similar to the climatology of the annual-mean SCF distribution, with high values distributed at high latitudes and high altitudes regions, but low values distributed in plains and low latitudes (Figure 8a). Moreover, changes in April–August averaged land surface albedo are highly consistent with SCF anomalies over the NH for the period 1982–2018, in which the correlation coefficient are positive in 78.68% of the entire study area (Figure 8b).

The interannual variability of April–August averaged land surface albedo and GLASS SCE-retrieved SCF shown consistent peaks and valleys for the period 1982–2018 (Figure 8c), with peaks occurred in year of 1992, 1996, and 2009, and valleys distributed in year of 2001, 2005, and 2016. In addition, both land surface albedo and SCF displayed significant decreasing trend between 1982 and 2018. The results of scatter plots further confirmed the tight correlation between land surface albedo calculated from CLARA-A2-SAL and SCF calculated from GLASS SCE, with r varies as 0.76 at the 95% significant level (Figure 8d). By comparison with independent land surface albedo, we found that the newly developed GLASS SCE is feasible in capturing long-term snow cover anomalies across the NH.

5 Discussion

The long-term snow cover across the NH has not been well documented owing to limited data availability. Compared with previous SCE products derived from AVHRR images, the development of GLASS SCE takes advantage of the consistent daily average surface reflectance and brightness temperatures from AVHRR-SR CDR, which reduced the systematic differences between individual AVHRR sensors including TIROS-N, NOAA-7, NOAA-9, NOAA-11, NOAA-14, NOAA-16, and NOAA-19, as well as the bias between AVHRR sensors and MODIS. Both binary snow mask and fractional snow cover are taken into consideration in the development of GLASS SCE. Compared with binary snow mask, fractional snow cover in each gridcell would provide better accuracy because of fragmented snow distributions over the NH. However, due to relatively coarse spatial resolution of AVHRR-SR CDR and complex topography over the NH, the endmembers within each gridcell vary over time, which limits the application of spectral unmixing algorithms among images with different times and locations. Thus, we developed binary snow mask instead of fractional snow cover products in the present study.

Although daily SCE dataset based on AVHRR images have been developed, such as Hori et al. (2017) and Naegeli et al. (2021b), the demand for longterm gap-free SCE records still cannot be fully satisfied caused by cloud contamination, swath coverage, warm bright surface features, and low illumination in daily AVHRR images and subsequent daily SCE products. Moreover, owing to shortage of satellite observations before 2000, gap-filling of daily SCE products is unachievable. In

https://doi.org/10.5194/essd-2021-279
Preprint. Discussion started: 16 December 2021

addition, the development of SCE with finer spatial resolution, such as high-resolution operational snow cover maps from Sentinel-2 and Landsat-8 data (Gascoin et al., 2019), cannot replace the role of longterm SCE in climate change studies. Therefore, aggregation of daily SCE to 8-day composite SCE is a reasonable solution to remove gaps in SCE products.

Due to incomplete spatial and temporal coverage, the validation of snow classification of daily NHSCE-D is difficult. Therefore, we employed three independent datasets including GHCN daily snow depth observations, 8-day MOD10C2 snow cover fraction, and CLARA-A2-SAL to verify the application accuracy of GLASS SCE in this study. The validation analysis of GLASS SCE by using GHCN daily snow depth stations displayed a general overestimated SCF values over the station-covered gridcells for the period 1982–2017. This phenomena was mainly caused by the coarse spatial resolution of the GLASS SCE, which provides the average SCF in pixel scale, which cannot totally catch and reflect the "ground truth" of SCF in specific spot location. Moreover, as shown in Figure 1, to meet the needs of long temporal coverage in the validation process, only 562 stations were selected in the analysis. The selected GHCN snow depth stations are not evenly distributed over the NH and most of the selected stations are located in middle latitudes and Europe. Therefore, this study also employed objective MOD10C2 in the validation analysis. The cross-comparison between GLASS SCE and MOD10C2 provides comparable spatial distribution over the NH for the period 2001–2019. In addition, the cross-comparison between GLASS SCE and CLARA-A2-SAL between 1982 and 2018 further confirmed the potential of GLASS SCE in climate change studies.

6 Data availability

The newly developed 39 year 8-day gap-free GLASS SCE data sets provides binary maps of snow cover for the NH from September 1981 to the December 2019. The data are freely available at https://doi.org/10.5281/zenodo.5775238 (Chen et al. 2021), which are organized by year and provided in GeoTIFF formats. The gridcells were flagged as "1" if covered by snow and 0 if no snow. This continual scale gap-free SCE product will beneficial snow cover and climate change applications, especially for years before 2000.

7 Conclusions

The extent of snow cover over the Northern Hemisphere is a vital indicator of climate change, and plays an irreplaceable role in climate model simulations. To meet the demands of longterm gap-free SCE dataset in climate change monitoring and forecasting, this study developed a 39 year consistent 8-day 0.05 degree gap-free SCE dataset over the NH for the period 1981–2019 based on the NOAA AVHRR-SR CDR and several contributory datasets. Using AVHRR-SR CDR as primary input dataset ensures the temporal consistent of GLASS SCE. Compared with published continental scale snow cover datasets, the newly developed GLASS SCE dataset has several advantages in snow cover studies over the NH, including long time series, finer spatial resolution (especially for years before 2000), and complete spatial coverage, compared with NOAA NHSSCE (low spatial resolution), Suomi-NPP and MODIS (short time span), as well as ESA SCFG and JASMES (incomplete coverage).

https://doi.org/10.5194/essd-2021-279
Preprint. Discussion started: 16 December 2021

Moreover, combination with two existing SCE products and aggregation daily SCE in 8-day interval improve the spatial integrity of GLASS SCE.

Compared with the 35-year averaged annual SCF (38.14± 8.19%) calculated from 562 GHCN snow depth observations for the period 1982–2017 (without 1994), the comparable results from GLASS SCE are higher (47.66 ± 15.76%) at the same time span, which indicate a overestimated SCF in the newly developed GLASS SCE. However, the validation by using 8-day MOD10C2 snow cover products for the period 2001–2019 indicated that the performance of GLASS SCE is comparable with MOD10C2. The annual SCF calculated from GLASS SCE and MOD10C2 are tightly correlated over the NH for the period 2001–2019, with correlation coefficient r being 0.97 at the 95% significant level, accompanied with RMSE and bias varies being 2.05% and 5.82%, respectively. Moreover, the cross-comparisons between the independent April–August averaged annual SCF calculated form GLASS SCE and land surface albedo calculated from CLARA-A2-SAL are highly correlated ($r = 0.76$, $p < 0.05$) for the period 1982–2018 which further demonstrates the reliability of GLASS SCE in climate change studies. Although some issues remain in GLASS NHSCE, such as overestimated overestimation of SCF compared with GHCN ground observations and MOD10C2. This long-term composite snow cover data set is still suited for studying seasonal snow cover over the NH and could presents a unique opportunity for climatological and hydrological studies on seasonal snow cover and snow-related model simulations across the NH for its long time span, relative finer spatial resolution, and complete spatial coverage. With the application of deep learning in snow cover detection, long-term, high-quality, and fine resolution fractional snow cover products are expected in the future.

Author contributions

XC and SL designed the research; XC and LH developed the methodological approach; XC, LH and CY organized the original data; XC and LH developed the gridded dataset. XC and CY performed the validation processes and performed the analysis and presentation of the results. XC and SL designed and wrote the manuscript with contribution from all co-authors.

Competing interests

The authors declare that they have no conflict of interest.

Acknowledgements

This work was jointly supported by the National Natural Science Foundation of China (No.42001377), the National Key Research and Development Program of China (No.2016YFA0600103), and the National Earth System Science Data Center of China at http://www.geodata.cn (No.2005DKA32300). Moreover, we would like to thank the NOAA's National Centers for Environmental Information for the online available Climate Data Record (CDR) of AVHRR Surface Reflectance, the National

Snow and Ice Data Center of United States for the online available MOD10C2 and IMS datasets, the ESA Snow Climate Change Initiative for the online available SCFG, the Earth Observation Research Center of the Japan Aerospace Exploration Agency for the online available JASMES, and the Satellite Application Facility on Climate Monitoring for the online available CLARA-A2-SAL. Meanwhile, we would like to thank all people fighting with COVID-19.

Financial support

This work was jointly supported by the National Natural Science Foundation of China (No.42001377), the National Key Research and Development Program of China (No.2016YFA0600103), and the National Earth System Science Data Sharing Infrastructure (No.2005DKA32300).

References

Barnett, T. P., Adam, J. C., and Lettenmaier, D. P.: Potential impacts of a warming climate on water availability in snow-dominated regions, Nature, 438, 303-309, https://doi.org/10.1038/nature04141, 2005.

Becker, J. J., Sandwell, D. T., Smith, W. H. F., Braud, J., Binder, B., Depner, J., Fabre, D., Factor, J., Ingalls, S., Kim, S. H., Ladner, R., Marks, K., Nelson, S., Pharaoh, A., Trimmer, R., Von Rosenberg, J., Wallace, G., and Weatherall, P.: Global Bathymetry and Elevation Data at 30 Arc Seconds Resolution: SRTM30_PLUS, Mar. Geodesy, 32, 355-371, https://doi.org/10.1080/01490410903297766, 2009.

Bojinski, S., Verstraete, M., Peterson, T. C., Richter, C., Simmons, A., and Zemp, M.: The Concept of Essential Climate Variables in Support of Climate Research, Applications, and Policy, Bull. Amer. Meteor. Soc., 95, 1431-1443, https://doi.org/10.1175/bams-d-13-00047.1, 2014.

Boos, W. R. and Kuang, Z.: Dominant control of the South Asian monsoon by orographic insulation versus plateau heating, Nature, 463, 218-222, https://doi.org/10.1038/nature08707, 2010.

Brodzik, M. J. and Armstrong, R.: Northern Hemisphere EASE-Grid 2.0 Weekly Snow Cover and Sea Ice Extent, Version 4, NASA National Snow and Ice Data Center Distributed Active Archive Center, https://doi.org/10.5067/P7O0HGJLYUQU, 2013.

Chen, C., Lakhankar, T., Romanov, P., Helfrich, S., Powell, A., and Khanbilvardi, R.: Validation of NOAA-Interactive Multisensor Snow and Ice Mapping System (IMS) by Comparison with Ground-Based Measurements over Continental United States, Remote Sens., 4, 1134-1145, https://doi.org/10.3390/rs4051134, 2012.

Chen, X. and Yang, Y.: Observed earlier start of the growing season from middle to high latitudes across the Northern Hemisphere snow-covered landmass for the period 2001–2014, Environ. Res. Lett., https://doi.org/10.1088/1748-9326/ab6d39, 2020.

Chen, X., Liang, S., and Cao, Y.: Satellite observed changes in the Northern Hemisphere snow cover phenology and the associated radiative forcing and feedback between 1982 and 2013, Environ. Res. Lett., 11, 084002, https://doi.org/10.1088/1748-9326/11/8/084002, 2016.

Chen, X., Yang, Y., Ma, Y., and Li, H.: Distribution and Attribution of Terrestrial Snow Cover Phenology Changes over the Northern Hemisphere during 2001–2020, Remote Sens., 13, 1843, https://doi.org/10.3390/rs13091843, 2021.

Chen, X., Liang, S., Cao, Y., He, T., and Wang, D.: Observed contrast changes in snow cover phenology in northern middle and high latitudes from 2001-2014, Sci. Rep., 5, 16820, https://doi.org/10.1038/srep16820, 2015.

Chen, X., Long, D., Liang, S., He, L., Zeng, C., Hao, X., and Hong, Y.: Developing a composite daily snow cover extent record over the Tibetan Plateau from 1981 to 2016 using multisource data, Remote Sens. Environ., 215, 284-299, https://doi.org/10.1016/j.rse.2018.06.021, 2018.

Chen, X., Liang, S., Yang, Y., He, L., and Yin, C.: A temporally consistent 8-day 0.05° gap-free snow cover extent dataset over the Northern Hemisphere for the period 1981–2019, zenodo, https://doi.org/10.5281/zenodo. 5775238, 2021.

Diffenbaugh, N. S., Scherer, M., and Ashfaq, M.: Response of snow-dependent hydrologic extremes to continued global warming, Nat. Clim. Chang., 3, 379-384, https://doi.org/10.1038/nclimate1732, 2013.

Dong, J., Zhang, G., Zhang, Y., and Xiao, X.: Reply to Wang et al.: Snow cover and air temperature affect the rate of changes in spring phenology in the Tibetan Plateau, Proc. Natl. Acad. Sci. U S A, 110, E2856-E2857, https://doi.org/10.1073/pnas.1306813110, 2013.

Estilow, T. W., Young, A. H., and Robinson, D. A.: A long-term Northern Hemisphere snow cover extent data record for climate studies and monitoring, Earth Syst. Sci. Data, 7, 137-142, https://doi.org/10.5194/essd-7-137-2015, 2015.

Flanner, M. G., Shell, K. M., Barlage, M., Perovich, D. K., and Tschudi, M. A.: Radiative forcing and albedo feedback from the Northern Hemisphere cryosphere between 1979 and 2008, Nat. Geosci., 4, 151-155, https://doi.org/10.1038/NGEO1062, 2011.

Franch, B., Vermote, E., Roger, J.-C., Murphy, E., Becker-Reshef, I., Justice, C., Claverie, M., Nagol, J., Csiszar, I., Meyer, D., Baret, F., Masuoka, E., Wolfe, R., and Devadiga, S.: A 30+ Year AVHRR Land Surface Reflectance Climate Data Record and Its Application to Wheat Yield Monitoring, Remote Sens., 9, 296, https://doi.org/10.3390/rs9030296, 2017.

Frei, A., Tedesco, M., Lee, S., Foster, J., Hall, D. K., Kelly, R., and Robinson, D. A.: A review of global satellite-derived snow products, Adv. Space Res., 50, 1007-1029, https://doi.org/10.1016/j.asr.2011.12.021, 2012.

Friedl, M. A. and Sulla-Menashe, D.: MCD12C1 MODIS/Terra+Aqua Land Cover Type Yearly L3 Global 0.05 Deg CMG V006, NASA EOSDIS Land Processes DAAC. https://doi.org/10.5067/MODIS/MCD12C1.006, Accessed on 30 June 2021, 2015.

Gascoin, S., Grizonnet, M., Bouchet, M., Salgues, G., and Hagolle, O.: Theia Snow collection: high-resolution operational snow cover maps from Sentinel-2 and Landsat-8 data, Earth Syst. Sci. Data, 11, 493-514, https://doi.org/10.5194/essd-11-493-2019, 2019.

https://doi.org/10.5194/essd-2021-279
Preprint. Discussion started: 16 December 2021

GCOS: Albedo: Essential Climate Variable (ECV) Factsheet. Available online: https://gcos.wmo.int/en/essential-climate-variables/albedo, Accessed on 15 September 2020, 2019a.

GCOS: Snow: Essential Climate Variable (ECV) Factsheet. Available online: https://gcos.wmo.int/en/essential-climate-variables/snow/, Accessed on 15 September 2020, 2019b.

Härer, S., Bernhardt, M., Siebers, M., and Schulz, K.: On the need for a time- and location-dependent estimation of the NDSI threshold value for reducing existing uncertainties in snow cover maps at different scales, The Cryosphere, 12, 1629-1642, https://doi.org/10.5194/tc-12-1629-2018, 2018.

Hall, D. K. and Riggs, G. A.: MODIS/Terra Snow Cover 8-Day L3 Global 0.05Deg CMG, Version 6, NASA National Snow and Ice Data Center Distributed Active Archive Center. https://doi.org/10.5067/MODIS/MOD10C2.006. Accessed on 12 July 2021, 2016.

Hall, D. K., Riggs, G. A., and Salomonson, V. V.: Development of Methods for Mapping Global Snow Cover Using Moderate Resolution Imaging Spectroradiometer Data, Remote Sens. Environ., 54, 127-140, https://doi.org/10.1016/0034-4257(95)00137-P, 1995.

Hansen, J., Ruedy, R., Sato, M., and Lo, K.: Global Surface Temperature Change, Rev. Geophys., 48, RG4004, https://doi.org/10.1029/2010rg000345, 2010.

Haynes, M. A., Kung, K.-J. S., Brandt, J. S., Yongping, Y., and Waller, D. M.: Accelerated climate change and its potential impact on Yak herding livelihoods in the eastern Tibetan plateau, Clim. Chang., 123, 147-160, https://doi.org/10.1007/s10584-013-1043-6, 2014.

Helfrich, S. R., McNamara, D., Ramsay, B. H., Baldwin, T., and Kasheta, T.: Enhancements to, and forthcoming developments in the Interactive Multisensor Snow and Ice Mapping System (IMS), Hydrol. Process., 21, 1576-1586, https://doi.org/10.1002/hyp.6720, 2007.

Henderson, G. R., Peings, Y., Furtado, J. C., and Kushner, P. J.: Snow–atmosphere coupling in the Northern Hemisphere, Nature Clim. Chang., 8, 954-963, https://doi.org/10.1038/s41558-018-0295-6, 2018.

Hock, R., Rasul, G., Adler, C., Cáceres, B., Gruber, S., Hirabayashi, Y., Jackson, M., Kääb, A., Kang, S., Kutuzov, S., A. Milner, Molau, U., Morin, S., Orlove, B., and Steltzer, H.: High Mountain Areas. In: IPCC Special Report on the Ocean and Cryosphere in a Changing Climate [M], In press, 2019.

Hori, M., Sugiura, K., Kobayashi, K., Aoki, T., Tanikawa, T., Kuchiki, K., Niwano, M., and Enomoto, H.: A 38-year (1978–2015) Northern Hemisphere daily snow cover extent product derived using consistent objective criteria from satellite-borne optical sensors, Remote Sens. Environ., 191, 402-418, https://doi.org/10.1016/j.rse.2017.01.023, 2017.

Immerzeel, W. W., Lutz, A. F., Andrade, M., Bahl, A., Biemans, H., Bolch, T., Hyde, S., Brumby, S., Davies, B. J., Elmore, A. C., Emmer, A., Feng, M., Fernández, A., Haritashya, U., Kargel, J. S., Koppes, M., Kraaijenbrink, P. D. A., Kulkarni, A. V., Mayewski, P., Nepal, S., Pacheco, P., Painter, T. H., Pellicciotti, F., Rajaram, H., Rupper, S., Sinisalo, A., Shrestha, A. B., Viviroli, D., Wada, Y., Xiao, C., Yao, T., and Baillie, J. E. M.: Importance and vulnerability of the world's water towers, Nature, https://doi.org/10.1038/s41586-019-1822-y, 2019.

Karlsson, K.-G., Anttila, K., Trentmann, J., Stengel, M., Fokke Meirink, J., Devasthale, A., Hanschmann, T., Kothe, S., Jääskeläinen, E., Sedlar, J., Benas, N., van Zadelhoff, G.-J., Schlundt, C., Stein, D., Finkensieper, S., Håkansson, N., and Hollmann, R.: CLARA-A2: the second edition of the CM SAF cloud and radiation data record from 34 years of global AVHRR data, Atmos. Chem. Phys., 17, 5809-5828, https://doi.org/10.5194/acp-17-5809-2017, 2017.

Kelly, R., Chang, A., Tsang, L., and James, F.: A Prototype AMSR-E Global Snow Area and Snow Depth Algorithm, IEEE Trans. Geosci. Remote Sens., 41, 230-242, https://doi.org/10.1109/TGRS.2003.809118, 2003.

Key, J. R., Mahoney, R., Liu, Y., Romanov, P., Tschudi, M., Appel, I., Maslanik, J., Baldwin, D., Wang, X., and Meade, P.: Snow and ice products from Suomi NPP VIIRS, J. Geophys. Res. Atmos., 118, 12,816-812,830, https://doi.org/10.1002/2013jd020459, 2013.

Khlopenkov, K. V. and Trishchenko, A. P.: SPARC: New Cloud, Snow, and Cloud Shadow Detection Scheme for Historical 1-km AVHHR Data over Canada, J. Atmos. Ocean Technol., 24, 322-343, https://doi.org/10.1175/jtech1987.1, 2007.

Kidder, S. Q.: A multispectral study of the St. Louis area under snow-covered conditions using NOAA-7 AVHRR data, Remote Sens. Environ., 22, 159-172, https://doi.org/10.1016/0034-4257(87)90056-3, 1987.

Liang, S., Wang, D., Cheng, J., He, T., Tao, X., Yao, Y., & , and Zhang, X.: Methodologies for Integrating Multiple High-Level Remotely Sensed Land Products, In Comprehensive Remote Sensing Vol. 2 Remote sensing data processing and analysis methodology. Oxford, UK: Elsevier, 278-317, 2018.

Liang, S., Cheng, J., Jia, K., Jiang, B., Liu, Q., Xiao, Z., Yao, Y., Yuan, W., Zhang, X., Zhao, X., and Zhou, J.: The Global Land Surface Satellite (GLASS) Product Suite, Bull. Amer. Meteor. Soc., 102, E323-E337, https://doi.org/10.1175/bams-d-18-0341.1, 2021.

Mallett, R. D. C., Stroeve, J. C., Tsamados, M., Landy, J. C., Willatt, R., Nandan, V., and Liston, G. E.: Faster decline and higher variability in the sea ice thickness of the marginal Arctic seas when accounting for dynamic snow cover, The Cryosphere, 15, 2429-2450, https://doi.org/10.5194/tc-15-2429-2021, 2021.

Menne, M. J., Durre, I., Vose, R. S., Gleason, B. E., and Houston, T. G.: An Overview of the Global Historical Climatology Network-Daily Database, J. Atmos. Oceanic Technol., 29, 897-910, https://doi.org/10.1175/jtech-d-11-00103.1, 2012.

Metsämäki, S., Pulliainen, J., Salminen, M., Luojus, K., Wiesmann, A., Solberg, R., Böttcher, K., Hiltunen, M., and Ripper, E.: Introduction to GlobSnow Snow Extent products with considerations for accuracy assessment, Remote Sens. Environ., 156, 96-108, https://doi.org/10.1016/j.rse.2014.09.018, 2015.

Muhammad, S. and Thapa, A.: An improved Terra–Aqua MODIS snow cover and Randolph Glacier Inventory 6.0 combined product (MOYDGL06*) for high-mountain Asia between 2002 and 2018, Earth Syst. Sci. Data, 12, 345-356, https://doi.org/10.5194/essd-12-345-2020, 2020.

Naegeli, K., Neuhaus, C., Salberg, A.-B., Schwaizer, G., Wiesmann, A., Wunderle, S., and Nagler, T.: ESA Snow Climate Change Initiative (Snow_cci): Daily global Snow Cover Fraction - viewable (SCFV) from AVHRR (1982–2019), version 1.0, NERC EDS Centre for Environmental Data Analysis, https://doi.org/10.5285/d9df331e346f4a50b18bcf41a64b98c7, Assessed on 12 May 2021, 2021a.

Naegeli, K., Neuhaus, C., Salberg, A. B., Schwaizer, G., Wiesmann, A., Wunderle, S., and Nagler, T.: ESA Snow Climate Change Initiative (Snow_cci): Daily global Snow Cover Fraction - snow on ground (SCFG) from AVHRR (1982–2019), version 1.0, NERC EDS Centre for Environmental Data Analysis, https://doi.org/10.5285/5484dc1392bc43c1ace73ba38a22ac56, Assessed on 12 May 2021, 2021b.

Nie, J., Stevens, T., Rittner, M., Stockli, D., Garzanti, E., Limonta, M., Bird, A., Ando, S., Vermeesch, P., Saylor, J., Lu, H., Breecker, D., Hu, X., Liu, S., Resentini, A., Vezzoli, G., Peng, W., Carter, A., Ji, S., and Pan, B.: Loess Plateau storage of Northeastern Tibetan Plateau-derived Yellow River sediment, Nat. commun., 6, 8511, https://doi.org/10.1038/ncomms9511, 2015.

NSIDC: IMS Daily Northern Hemisphere Snow and Ice Analysis at 1 km, 4 km, and 24 km Resolutions, Version 1, Boulder, Colorado USA. National Snow and Ice Data Center. https://doi.org/10.7265/N52R3PMC, Accessed on 10 January 2021, 2008.

NSIDC: State of the Cryosphere: Northern Hemisphere Snow, Available online: https://nsidc.org/cryosphere/sotc/snow_extent.html, Assessed on 08 July 2021, 2019.

Peltoniemi, M., Aurela, M., Böttcher, K., Kolari, P., Loehr, J., Karhu, J., Linkosalmi, M., Tanis, C. M., Tuovinen, J.-P., and Arslan, A. N.: Webcam network and image database for studies of phenological changes of vegetation and snow cover in Finland, image time series from 2014 to 2016, Earth Syst. Sci. Data, 10, 173-184, https://doi.org/10.5194/essd-10-173-2018, 2018.

Pulliainen, J.: Mapping of snow water equivalent and snow depth in boreal and sub-arctic zones by assimilating space-borne microwave radiometer data and ground-based observations, Remote Sens. Environ., 101, 257-269, https://doi.org/10.1016/j.rse.2006.01.002, 2006.

Pulliainen, J., Luojus, K., Derksen, C., Mudryk, L., Lemmetyinen, J., Salminen, M., Ikonen, J., Takala, M., Cohen, J., Smolander, T., and Norberg, J.: Patterns and trends of Northern Hemisphere snow mass from 1980 to 2018, Nature, 581, 294-298, https://doi.org/10.1038/s41586-020-2258-0, 2020.

Pulliainen, J., Aurela, M., Laurila, T., Aalto, T., Takala, M., Salminen, M., Kulmala, M., Barr, A., Heimann, M., Lindroth, A., Laaksonen, A., Derksen, C., Makela, A., Markkanen, T., Lemmetyinen, J., Susiluoto, J., Dengel, S., Mammarella, I., Tuovinen, J. P., and Vesala, T.: Early snowmelt significantly enhances boreal springtime carbon uptake, Proc. Natl. Acad. Sci. U S A, 114, 11081-11086, https://doi.org/10.1073/pnas.1707889114, 2017.

Qin, Y., Abatzoglou, J. T., Siebert, S., Huning, L. S., AghaKouchak, A., Mankin, J. S., Hong, C., Tong, D., Davis, S. J., and Mueller, N. D.: Agricultural risks from changing snowmelt, Nature Clim. Chang., 10, 459-465, https://doi.org/10.1038/s41558-020-0746-8, 2020.

Qu, X. and Hall, A.: On the persistent spread in snow-albedo feedback, Clim. Dyn., 42, 69–81, https://doi.org/10.1007/s00382-013-1774-0, 2014.

Riihelä, A., Manninen, T., and Laine, V.: Observed changes in the albedo of the Arctic sea-ice zone for the period 1982–2009, Nat. Clim. Chang., 3, 895-898, https://doi.org/10.1038/nclimate1963, 2013.

Robinson, D. A., Estilow, T. W., and Program, N. C.: NOAA Climate Data Record (CDR) of Northern Hemisphere (NH) Snow Cover Extent (SCE), Version 1, NOAA National Centers for Environmental Information., https://doi.org/10.7289/V5N014G9, Accessed on 10 January 2021, 2012.

Robinson, D. A., Hall, D. K., and Mote, T. L.: MEaSUREs Northern Hemisphere Terrestrial Snow Cover Extent Daily 25km EASE-Grid 2.0, Version 1., https://doi.org/10.5067/MEASURES/CRYOSPHERE/nsidc-0530.001, Accessed on 10 January 2021, 2014.

Thackeray, C. W. and Fletcher, C. G.: Snow albedo feedback: Current knowledge, importance, outstanding issues and future directions, Prog. Phys. Geogr., https://doi.org/10.1177/0309133315620999, 2016.

Vermote, E., Chris, J., Ivan, C., Jeff, E., Ranga, M., Frederic, B., Ed, M., Robert, W., Martin, C., and Program, N. C.: NOAA Climate Data Record (CDR) of AVHRR Surface Reflectance, Version 5., NOAA National Centers for Environmental Information, https://doi.org/10.7289/V53776Z4, Accessed on 10 December 2020. 2019.

Wang, X., Wu, C., Peng, D., Gonsamo, A., and Liu, Z.: Snow cover phenology affects alpine vegetation growth dynamics on the Tibetan Plateau: Satellite observed evidence, impacts of different biomes, and climate drivers, Agr. Forest. Meteorol., 256-257, 61-74, https://doi.org/10.1016/j.agrformet.2018.03.004, 2018.

WMO: WMO Statement on the State of the Global Climate in 2019, Available online: https://public.wmo.int/en/resources/library/wmo-statement-state-of-global-climate-2019, Accessed on 15 April 2021, 2020.

Xu, W., Ma, L., Ma, M., Zhang, H., and Yuan, W.: Spatial–Temporal Variability of Snow Cover and Depth in the Qinghai–Tibetan Plateau, J. Clim., 30, 1521-1533, https://doi.org/10.1175/jcli-d-15-0732.1, 2017.

Yang, J., Gong, P., Fu, R., Zhang, M., Chen, J., Liang, S., Xu, B., Shi, J., and Dickinson, R.: The role of satellite remote sensing in climate change studies, Nat. Clim. Chang., 3, 875-883, https://doi.org/10.1038/nclimate1908, 2013.

Yuan, W., Xu, W., Ma, M., Chen, S., Liu, W., and Cui, L.: Improved snow cover model in terrestrial ecosystem models over the Qinghai–Tibetan Plateau, Agr. Forest. Meteorol., 218-219, 161-170, https://doi.org/10.1016/j.agrformet.2015.12.004, 2016.

Zhang, H., Zhang, F., Zhang, G., Che, T., Yan, W., Ye, M., and Ma, N.: Ground-based evaluation of MODIS snow cover product V6 across China: Implications for the selection of NDSI threshold, Sci. Total Environ., 651, 2712-2726, https://doi.org/10.1016/j.scitotenv.2018.10.128, 2019.

Zhou, H., Aizen, E., and Aizen, V.: Deriving long term snow cover extent dataset from AVHRR and MODIS data: Central Asia case study, Remote Sens. Environ., 136, 146-162, https://doi.org/10.1016/j.rse.2013.04.015, 2013.

https://doi.org/10.5194/essd-2021-279
Preprint. Discussion started: 16 December 2021

Open Access Earth System Science Data Discussions

Figures

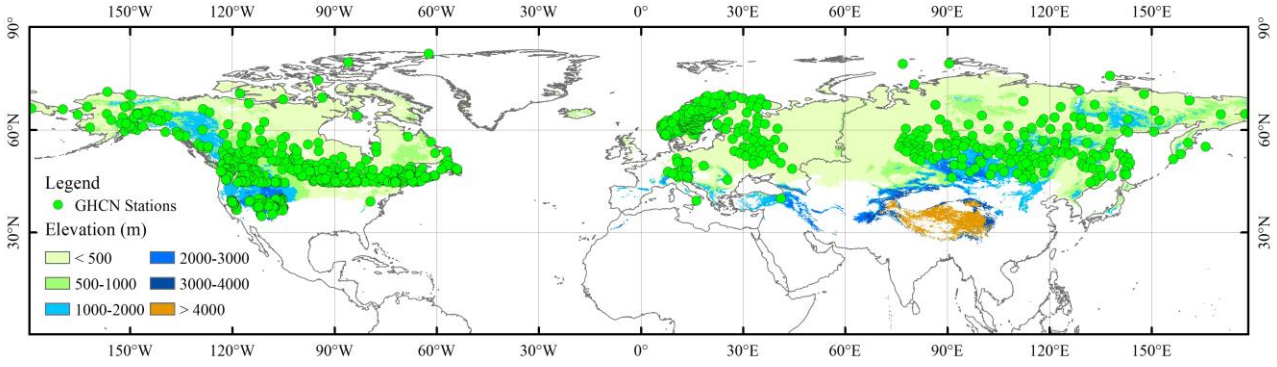

620

Figure 1. Distribution of the 562 GHCN snow depth observations over the Northern Hemisphere.

https://doi.org/10.5194/essd-2021-279
Preprint. Discussion started: 16 December 2021

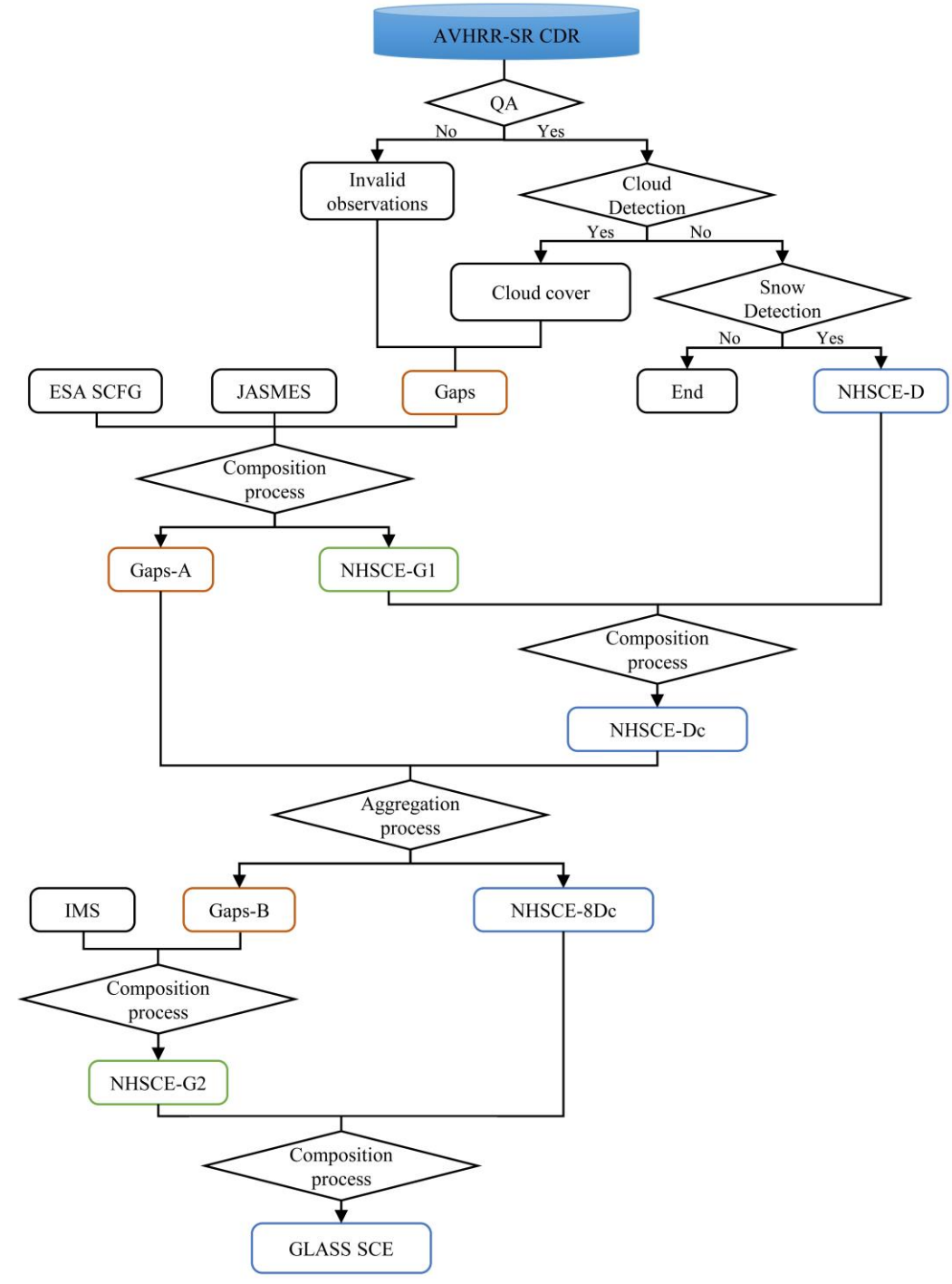

Figure 2. Flowchart of the 8-day gap-free terrestrial snow cover extent over the Northern hemisphere (GLASS SCE) generation using the AVHRR-SR CDR and several existing SCE dataset.

https://doi.org/10.5194/essd-2021-279
Preprint. Discussion started: 16 December 2021

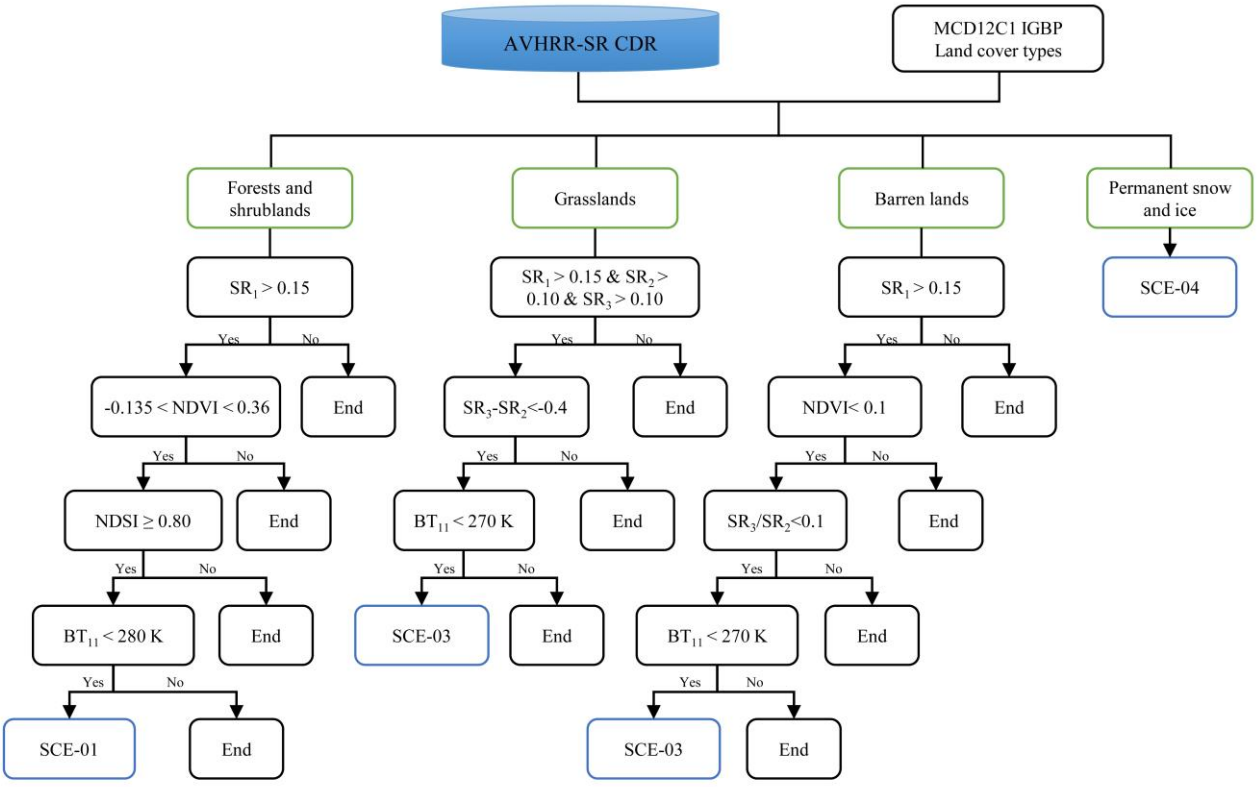

Figure 3. Decision tree and threshold values for snow cover detection using AVHRR surface reflectance CDR. NDVI = (SR_2-SR_1) / (SR_2+SR_1). NDSI= (SR_1-SR_3) / (SR_1+SR_3).

https://doi.org/10.5194/essd-2021-279
Preprint. Discussion started: 16 December 2021

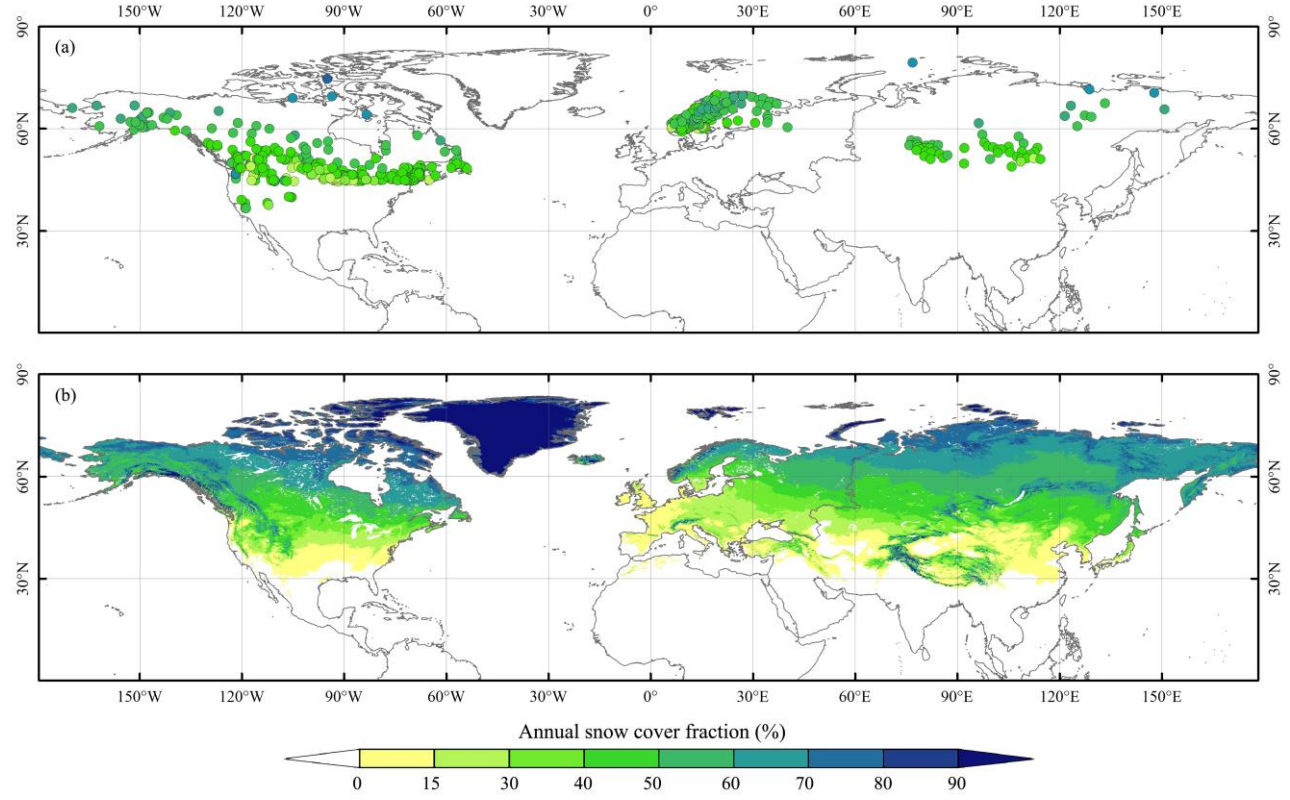

Figure 4. 35-year climatology of snow cover fraction (%) calculated from (a) 562 GHCN snow depth observations, and (b) the GLASS SCE across the Northern Hemisphere for the period 1982–2017 (without 1994).

https://doi.org/10.5194/essd-2021-279
Preprint. Discussion started: 16 December 2021

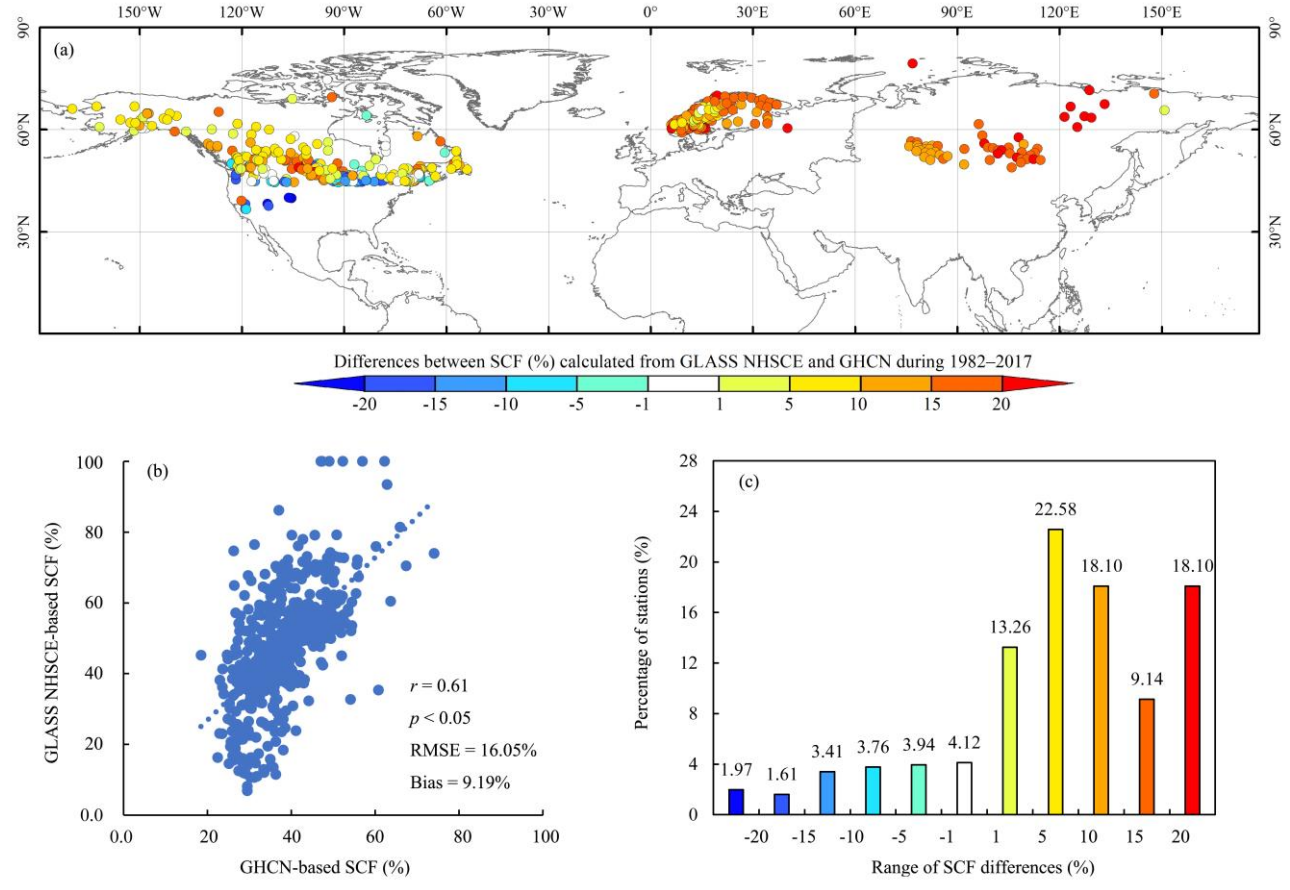

Figure 5. (a) Differences between 35-year averaged annual SCF calculated from GLASS SCE and GHCN snow depth observations over the NH for the period 1982–2017 (without 1994). (b) Scatter plots between GLASS SCE-retrieved annual SCF and GHCN-observed annual SCF over the NH for the period 1982–2017 (without 1994). (c) Range of SCF differences. The differences were given by GLASS SCE-retrieved annual SCF minus GHCN-observed annual SCF.

https://doi.org/10.5194/essd-2021-279
Preprint. Discussion started: 16 December 2021

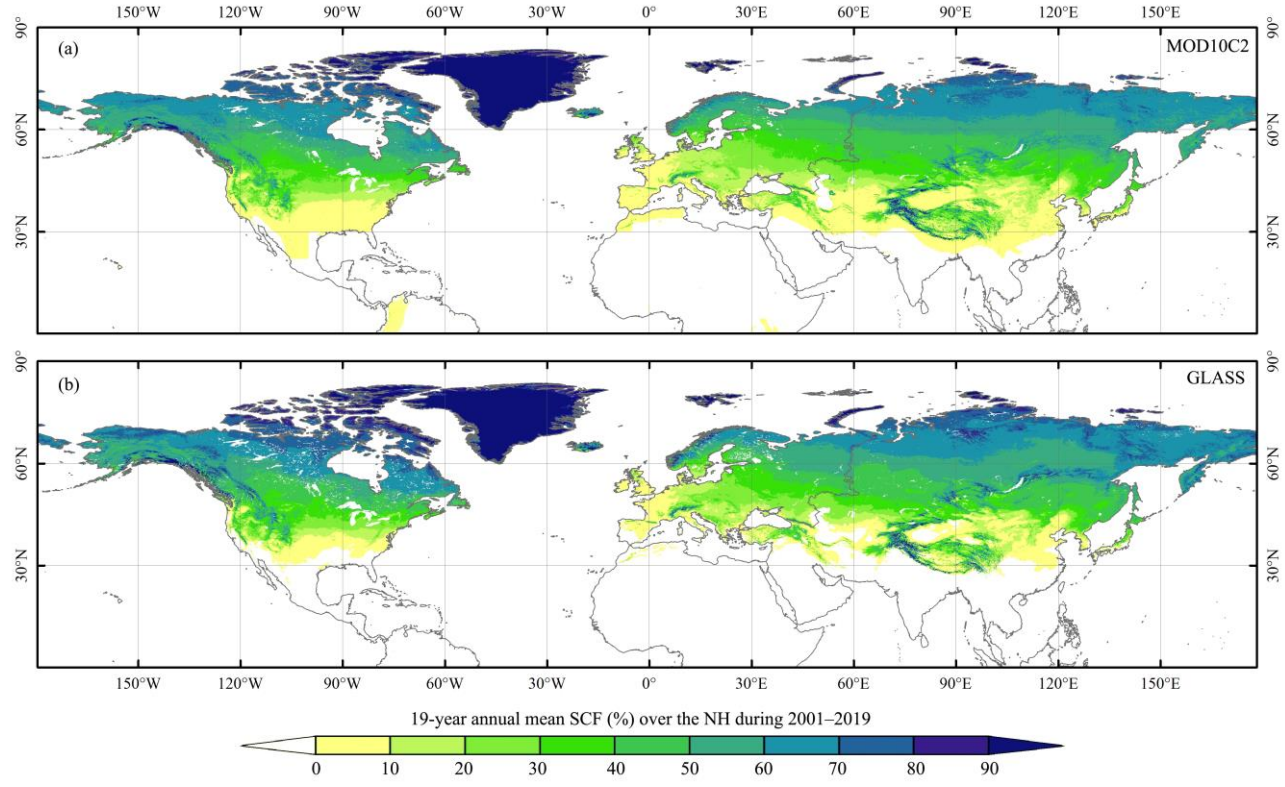

Figure 6. Spatial distribution of 19-year averaged snow cover fraction over the Northern Hemisphere for the period 2001–2019 calculated from (a) MOD10C2 and (b) GLASS SCE.

https://doi.org/10.5194/essd-2021-279
Preprint. Discussion started: 16 December 2021

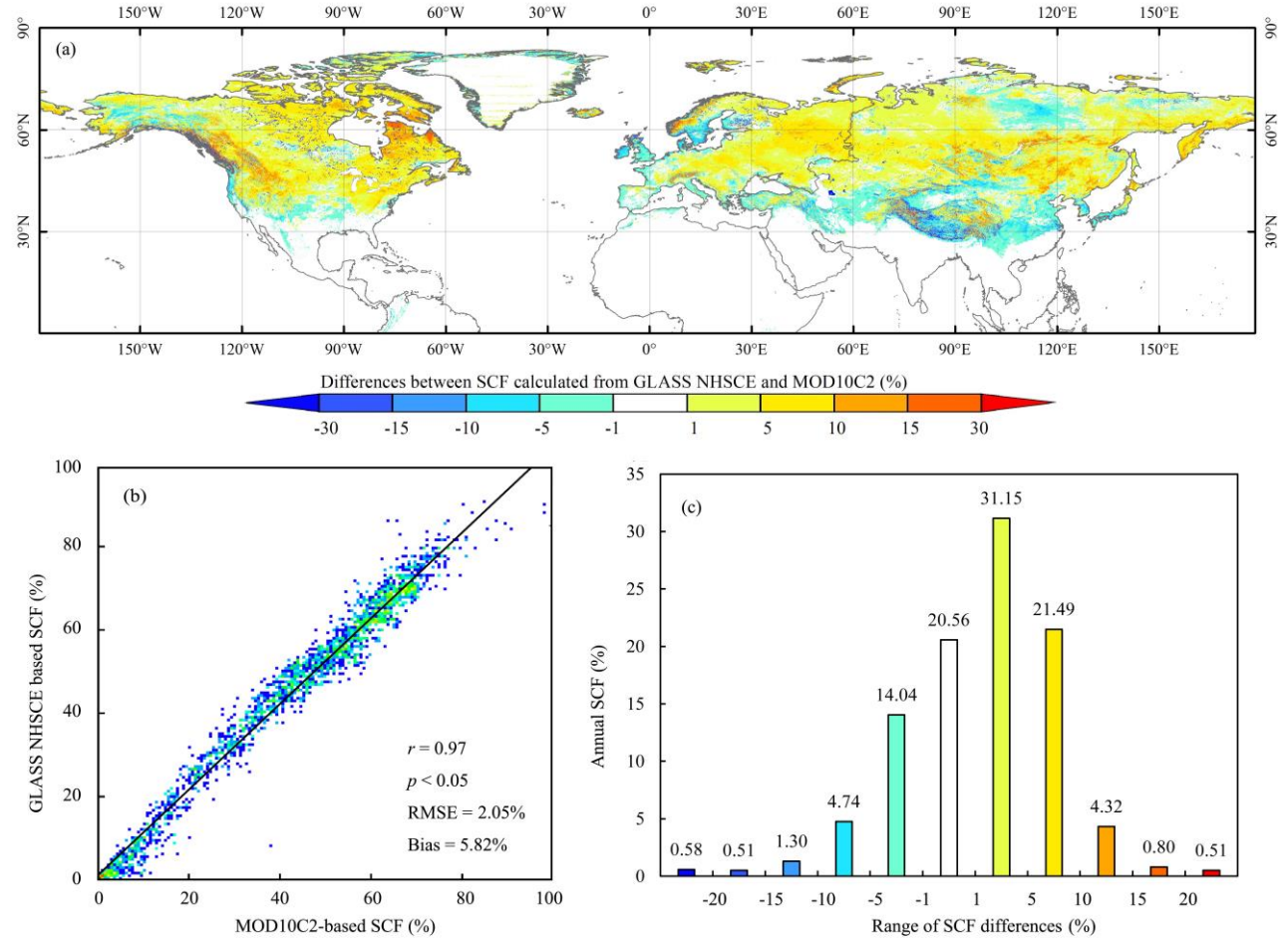

640 **Figure 7. (a) Spatial distribution of differences between 19-year averaged annual SCF calculated from GLASS SCE and MOD10C2 over the NH for the period 2001–2019. (b) Scatter plots between 19-year averaged annual SCF calculated from GLASS SCE and MOD10C2 for the period 2001–2019. (c) Range of 19-year annual SCF differences calculated from GLASS SCE and MOD10C2 for the period 2001–2019. The differences were given by GLASS SCE-retrieved annual SCF minus MOD10C2-based SCF annual SCF.**

https://doi.org/10.5194/essd-2021-279
Preprint. Discussion started: 16 December 2021

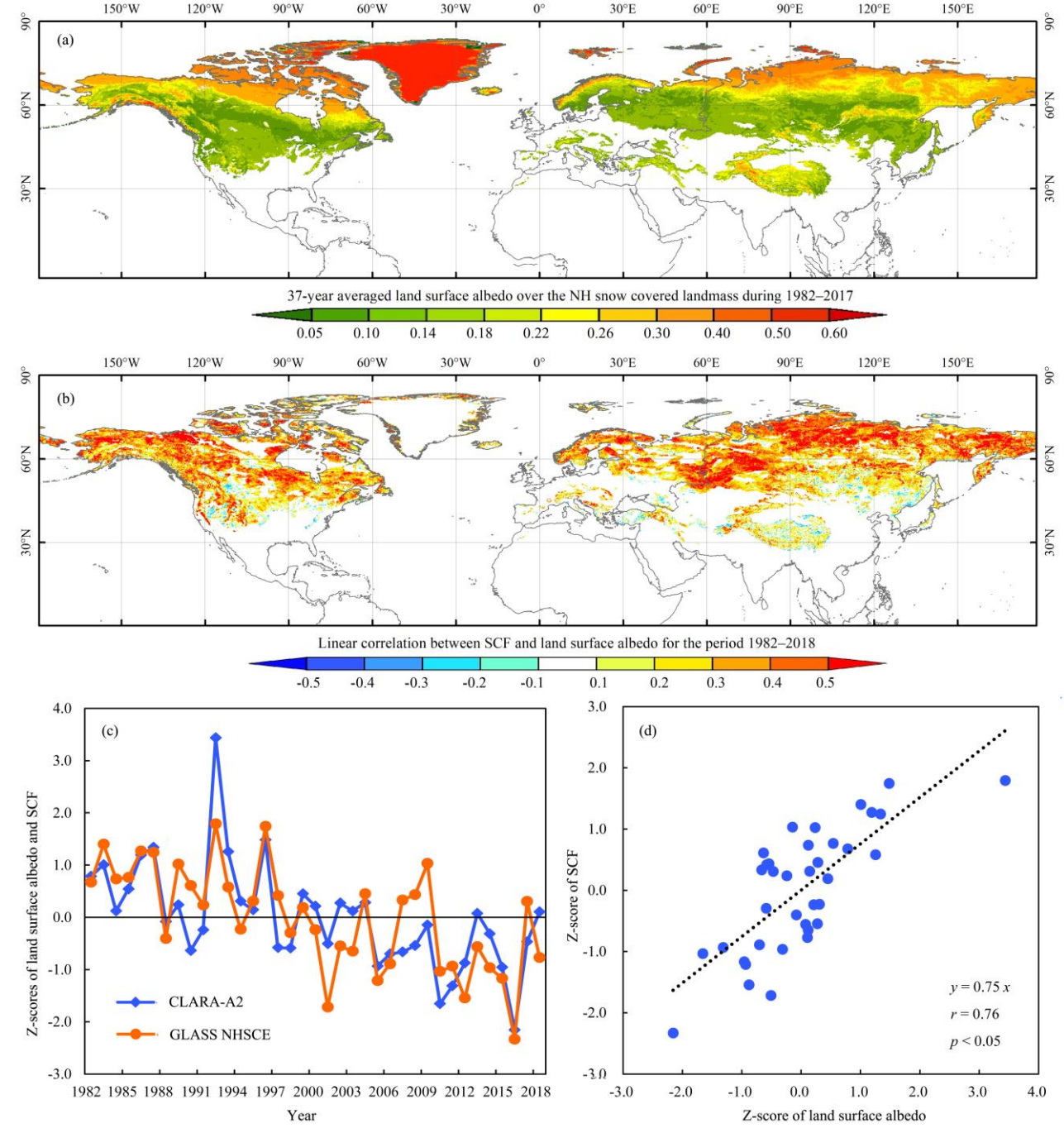

Figure 8. (a) 37-year mean of April–August averaged land surface albedo over the Northern Hemisphere for the period 1982–2018. (b) Linear correlation coefficients between April–August averaged land surface albedo and SCF over the Northern Hemisphere for the period 1982–2018. (c) Z-score of interannual variability of April–August averaged land surface albedo and SCF or the period 1982–2018. (d) Scatter plots between z-scores of April–August averaged land surface albedo and SCF or the period 1982–2018.

https://doi.org/10.5194/essd-2021-279
Preprint. Discussion started: 16 December 2021

Open Access Earth System Science Data Discussions

Tables

Table 1. Published continental scale snow cover dataset

Datasets	Spatial resolution	Temporal resolution	Time span	Spatially integrated	References
NOAA NHSCE-CDR	190.6 km	Weekly	1966–1999.05	Yes	Robinson et al. (2012) and Estilow et al. (2015)
		Daily	1999.06–Present	Yes	
NHSSCE	25 km	Weekly	1980.09–Present	Yes	Brodzik and Armstrong (2013)
MEaSUREs NHSCE	25km	Daily	1999.01–2012.12	Yes	Robinson et al. (2014)
IMS	1 km	Daily	2014.12–Present	Yes	Nsidc (2008)
	4 km	Daily	2004.02–Present	Yes	
	24 km	Daily	1997.02–Present	Yes	
JASMES	5 km	Daily	1978.11–2019.12	No	Hori et al. (2017)
MODIS CMG	5 km	Daily	2000.01–Present	No	Hall et al. (1995)
		8-day			
		Monthly			
VIIRS CMG	5 km	Daily	2012.01–Present	No	Key et al. (2013)
ESA Snow CCI SCFG	5 km	Daily	1982.01–2019.06	No	Naegeli et al. (2021b)
ESA Snow CCI SCFV					Naegeli et al. (2021a)
GlobSnow SE	1 km	Daily	1995.06–2012.04	No	Pulliainen (2006)

Table 2. Summary of spectral bands of CDR of AVHRR-SR CDR.

Bands	Wavelength (μm)	Description
1	0.58–0.68	Surface Reflectance at 0.64 μm (SR_1)
2	0.725–1.00	Surface Reflectance at 0.86 μm (SR_2)
3	3.55–3.93	Surface Reflectance at 3.75 microns (SR_3)
4	3.55–3.93	Brightness Temperature at 3.75 microns (BT_{37})
5	10.30–11.30	Brightness Temperature at 11.0 microns (BT_{11})
6	11.50–12.50	Brightness Temperature at 12.0 microns (BT_{12})
7	-	quality control flag

https://doi.org/10.5194/essd-2021-279
Preprint. Discussion started: 16 December 2021

Table 3. Summary of datasets used in GLASS SCE generation.

Variable	Datasets	Spatial resolution	Temporal resolution	Time span	References
Surface reflectance	AVHRR-SR CDR	0.05°	Daily	1981–2019	Vermote et al. (2019)
Land cover types	MCD12C1	0.05°	Yearly	2019	Friedl and Sulla-Menashe (2015)
Elevation	SRTM30	1-km	–		Becker et al. (2009)
Snow cover	JASMES	0.05°	Daily	1981–2019	Hori et al. (2017)
	IMS	4-km	Daily	2005–2019	NSIDC (2008)
	ESA SCFG	0.05°	Daily	1982–2019	Naegeli et al. (2021b)
	MOD10C2	0.05°	8-Day	2000–2019	Hall and Riggs (2016)
Snow depth	GHCN	–	Daily	1982–2017	Menne et al. (2012)
Surface albedo	CLARA-A2-SAL	0.25°	5-Day	1978–2015	Karlsson et al. (2017)